

STAR FORMATION IN ULTRALUMINOUS INFRARED GALAXIES PROBED WITH *AKARI* NEAR-INFRARED SPECTROSCOPY

KENICHI YANO^{1, 2}, TAKAO NAKAGAWA², NAOKI ISOBE^{2, 3}, AND MAI SHIRAHATA²

Draft version October 13, 2016

ABSTRACT

We conducted systematic observations of the H I Br α line (4.05 μ m) and the polycyclic aromatic hydrocarbon (PAH) feature (3.3 μ m) in 50 nearby ($z < 0.3$) ultraluminous infrared galaxies (ULIRGs) with *AKARI*. The Br α line is predicted to be the brightest among the H I lines under high dust-extinction conditions ($A_V > 15$ mag). The Br α line traces ionizing photons from OB stars and so is used as an indicator of star formation on the assumption of the initial mass function. We detected the Br α line in 33 ULIRGs. The luminosity of the line ($L_{\text{Br}\alpha}$) correlates well with that of the 3.3 μ m PAH emission ($L_{3.3}$). Thus we utilize $L_{3.3}$ as an indicator of star formation in fainter objects where the Br α line is undetected. The mean $L_{\text{Br}\alpha}/L_{\text{IR}}$ ratio in LINERs/Seyferts is significantly lower than that in H II galaxies. This difference is reconfirmed with the $L_{3.3}/L_{\text{IR}}$ ratio in the larger sample (46 galaxies). Using the ratios, we estimate that the contribution of starburst in LINERs/Seyferts is $\sim 67\%$, and active galactic nuclei contribute to the remaining $\sim 33\%$. However, comparing the number of ionizing photons, $Q_{\text{Br}\alpha}$, derived from $L_{\text{Br}\alpha}$ with that, Q_{IR} , expected from star formation rate required to explain L_{IR} , we find that the mean $Q_{\text{Br}\alpha}/Q_{\text{IR}}$ ratio is only $55.5 \pm 7.5\%$ even in H II galaxies which are thought to be energized by pure starburst. This deficit of ionizing photons traced by the Br α line is significant even taking heavy dust extinction into consideration. We propose that dust within H II regions absorbs a significant fraction of ionizing photons.

Keywords: galaxies: active — galaxies: nuclei — galaxies: star formation — infrared: galaxies

1. INTRODUCTION

Ultraluminous infrared galaxies (ULIRGs) radiate most ($\geq 90\%$) of their extremely large, quasar-like luminosities ($> 10^{12}L_{\odot}$) as infrared dust emission (Sanders et al. 1988). The possible energy source of their enormous infrared luminosity is starburst activities and/or active galactic nuclei (AGN). Morphologically, most ULIRGs exhibit merger features. Thus, ULIRGs are thought to be dust-enshrouded quasars formed through the merger processes, eventually shedding their dust to evolve into quasars or massive ellipticals (e.g., Sanders et al. 1988; Sanders & Mirabel 1996). Understanding whether the dust-obscured energy source of ULIRGs is dominated by starburst or AGN is therefore important to investigate this merger-driven evolutionary scenario.

To identify the energy source of galaxies, optical line ratios have been used to classify galaxies according to the excitation mechanism (e.g., Kim et al. 1998). This optical classification method was promoted by Baldwin et al. (1981), and later modified by Veilleux & Osterbrock (1987). On the basis of two-dimensional line-intensity ratios, such as [O III] $\lambda 5007/\text{H}\beta$ vs [N II] $\lambda 6583/\text{H}\alpha$, galaxies are mainly classified into three categories; H II galaxies, Seyferts, and LINERs. The emission lines are mainly excited by starburst and AGN in H II galaxies and Seyferts, respectively. The line excitation mechanisms in LINERs are not clear and still under debate

(e.g., see a review by Ho 2008). However, in ULIRGs, it is difficult to distinguish starburst and AGN through optical studies because of their high dust extinction. To avoid this problem, many attempts have been made to reveal dust-obscured energy sources with infrared observations.

Using near-infrared observations with *AKARI*, Imanishi et al. (2008, 2010b) found dust-obscured AGN signatures in a significant fraction of ULIRGs that were optically classified as non-Seyferts. From observations using *ISO* (e.g., Genzel et al. 1998) and *Spitzer* (e.g., Veilleux et al. 2009), the fractional contributions of starburst and AGN as the energy sources in ULIRGs have been estimated with less dust extinction bias. Their results of infrared observations, however, rely largely on empirical relations. For instance, many of them use the polycyclic aromatic hydrocarbon (PAH) feature as an indicator of starburst activities. PAH is thought to be excited by UV photons from OB stars; PAH emits fluorescent light at infrared wavelengths, but its emission mechanisms are very complex (Draine 2003). PAH emission has not been theoretically related to the number of UV photons from OB stars. Thus, quantitative discussion about the contribution of starburst or AGN is difficult on the basis of these observations.

To quantitatively investigate the energy sources of ULIRGs, we focus on the near-infrared hydrogen recombination line Br α ($n : 5 \rightarrow 4$, $\lambda_{\text{rest}} = 4.05 \mu\text{m}$). Since hydrogen is the simplest element, the number of ionizing photons from OB stars is calculated from the fluxes of hydrogen recombination lines on the basis of the photoionization model in the case B (Osterbrock & Ferland 2006). Star formation rates (SFRs) can then be estimated from the number of ionizing photons on the as-

¹ Department of Physics, Graduate School of Science, The University of Tokyo, 7-3-1 Hongo, Bunkyo-ku, Tokyo 113-0033, Japan

² Institute of Space and Astronautical Science, Japan Aerospace Exploration Agency, 3-1-1 Yoshinodai, Sagami-hara, Kanagawa 252-5210, Japan

³ Department of Physics, Tokyo Institute of Technology, 2-12-1 Ookayama, Meguro-ku, Tokyo 152-8550, Japan

sumption of the initial mass function (e.g., Kennicutt & Evans 2012). Thus, we can theoretically estimate the strength of starburst activities with hydrogen recombination lines. Owing to its near-infrared wavelength, the observed flux of the Br α line is predicted to be the highest among hydrogen recombination lines (i.e., H α or Pa α lines) in the conditions of high dust extinction (visual extinction $A_V > 15$ mag) which is expected in ULIRGs (e.g., Genzel et al. 1998). Therefore, the Br α line is the most suitable for probing starburst activities in ULIRGs.

With the unique wavelength coverage of the near-infrared 2.5–5.0 μm spectroscopy of *AKARI* (Murakami et al. 2007; Onaka et al. 2007), we succeed in systematically observing the Br α line in ULIRGs, whose wavelength is difficult to be accessed from ground-based telescopes. The *AKARI* near-infrared spectroscopy also has the unique capability to simultaneously observe the 3.3 μm PAH emission and the Br α line. The 3.3 μm PAH emission is stronger than the Br α line (Imanishi et al. 2008, 2010b), and hence, its luminosity can be used as an indicator of star formation for fainter objects if we calibrate it with the Br α line luminosity.

By comparing the Br α line (or the 3.3 μm PAH emission) luminosity with the total infrared luminosity, we quantitatively investigate the dust-obscured energy sources in ULIRGs. We assume that the Br α line luminosity is proportional to the strength of the starburst activity, i.e., SFRs. On the other hand, the total infrared luminosity has contributions from the starburst and the AGN. Thus, the ratio of the Br α line luminosity to the total infrared luminosity is expected to be an indicator of the contribution of starburst to the total infrared luminosity. In Section 2, we present our targets, observations, and data reduction method. Resulting spectra and measured Br α line fluxes are presented in Section 3. We utilize the Br α line and the 3.3 μm PAH emission as indicators of star formation and show a result of comparisons with the total infrared luminosity in there. Then, in Section 4, we discuss the contribution of starburst to the total energy from ULIRGs by comparing the Br α line and 3.3 μm PAH emission luminosities with the total infrared luminosity. We summarize our study in Section 5. Throughout this paper, we assume that the universe is flat with $\Omega_M = 0.27$, $\Omega_\Lambda = 0.73$, and $H_0 = 70.4 \text{ km s}^{-1} \text{ Mpc}^{-1}$ (Komatsu et al. 2011).

2. OBSERVATION AND DATA REDUCTION

2.1. Targets

Our targets are selected from the *AKARI* mission program “Evolution of ultraluminous infrared galaxies and active galactic nuclei” (AGNUL; P.I. T. Nakagawa), which aimed to investigate the connection between ULIRGs and AGN. The AGNUL program conducted systematic near-infrared spectroscopic observations of ULIRGs in the local universe. Among the archived data of AGNUL, we focus on the observations conducted during the liquid-He cool holding period (2006 May 8–2007 August 26). As a result, 50 near-infrared grism spectroscopic observations of ULIRGs are selected and used for this study. Table 1 summarizes the observation log.

The spectra of all the targets have been reported by Imanishi et al. (2008, 2010b). The 3.3 μm PAH feature

in these galaxies is closely investigated in their papers, but the Br α line is not discussed in detail. Thus, we further reduced the spectra to systematically derive the Br α line fluxes in the sample for the first time, while the 3.3 μm PAH emission fluxes and optical classifications of the galaxies are taken from Imanishi et al. (2008, 2010b). In addition, Table 2 summarizes the basic information, such as redshifts and *IRAS*-based total infrared luminosities (L_{IR}) of our target ULIRGs.

2.2. Spectral Analysis

The near-infrared spectroscopic observations were conducted with the InfraRed Camera (IRC) infrared spectrograph (Onaka et al. 2007) onboard the *AKARI* infrared satellite (Murakami et al. 2007). The 1×1 arcmin² window is used to avoid source overlap. The pixel scale of the *AKARI* IRC is $1''.46 \times 1''.46$. We used the NG grism mode (Onaka et al. 2007) to obtain a 2.5–5.0 μm spectrum. The NG grism has a dispersion of $9.7 \times 10^{-3} \mu\text{m pix}^{-1}$ and an effective spectral resolution of $\lambda/\delta\lambda \sim 120$ at 3.6 μm for a point source. We employed the observing mode of IRC04, in which one pointing comprised 8 or 9 independent frames. Thus, though we assigned only one pointing for each ULIRG, the effects of cosmic ray hits were removed. The total net on-source exposure time is ~ 6 min for each ULIRG.

The data were processed using “IRC Spectroscopy Toolkit Version 20110114,” the standard IDL toolkit prepared for the reduction of *AKARI* IRC spectra (Ohyama et al. 2007). Each frame was dark-subtracted, linearity-corrected, and flat-field corrected. Wavelength and flux calibrations were also made within this toolkit. The wavelength calibration accuracy is taken to be ~ 1 pixel or $\sim 10^{-2} \mu\text{m}$ (Ohyama et al. 2007). The absolute flux calibration accuracy is $\sim 10\%$ at the central wavelength of the spectra, and can be as large as $\sim 20\%$ at the edge of the spectra (Ohyama et al. 2007). We estimated a spatial extension of the object by stacking the spectrum along the spatial direction (i.e., perpendicular to the dispersion direction) for each source. The measured full width at half maximum (FWHM) of the spatial profile is typically ~ 4 –5 pixel, which is consistent with the size of the point spread function of *AKARI* IRC in spectroscopic mode (Lorente et al. 2008). We adopted an aperture width of 5 pixel ($= 7''.3$) along the spatial direction for the spectrum extraction for each ULIRG. Smoothing with a boxcar kernel of 3 pixel in the dispersion direction was applied to each spectrum.

2.3. Line Fitting

The Br α line at rest-frame wavelength of $\lambda_{\text{rest}} = 4.05 \mu\text{m}$ was fitted with a linear continuum and a single Gaussian profile in each spectrum. The free parameters are the offset and the slope of the linear continuum, the normalization of the Gaussian profile, and the central wavelength. The line width is fixed at the spatial width of each object (FWHM ~ 4 –5 pixel). Here, we assumed that the spectral resolution is determined by the size of each object because the observations employ slitless spectroscopy, and the intrinsic line widths are narrower than the $\sim 3000 \text{ km s}^{-1} \Delta v$ resolution. The range of wavelengths used for the fitting was determined to satisfactorily reproduce the continuum emission and is typically

Table 1
Observation Log of ULIRGs.

Object Name	Observation ID	Observation Date
IRAS 00183–7111	1100137.1	2007 May 2
IRAS 00456–2904	1100221.1	2007 Jun 19
IRAS 00482–2721	1100036.1	2006 Dec 21
IRAS 01199–2307	1100209.1	2007 Jul 1
IRAS 01298–0744	1100226.1	2007 Jul 10
IRAS 01355–1814	1100018.1	2007 Jan 6
IRAS 01494–1845	1100215.1	2007 Jul 10
IRAS 01569–2939	1100225.1	2007 Jul 7
IRAS 02480–3745	1100030.1	2007 Jan 14
IRAS 03209–0806	1100210.1	2007 Aug 8
IRAS 03521+0028	1100200.1	2007 Aug 19
IRAS 04074–2801	1100201.1	2007 Aug 14
IRAS 04313–1649	1100031.1	2007 Feb 22
IRAS 05020–2941	1100003.1	2007 Feb 28
IRAS 05189–2524	1100129.1	2007 Mar 8
IRAS 06035–7102	1100130.1	2007 Mar 11
IRAS 08572+3915	1100049.1	2006 Oct 29
IRAS 08591+5248	1100121.1	2007 Apr 21
IRAS 09320+6134 (UGC 5101)	1100134.1	2007 Apr 22
IRAS 09463+8141	1100004.1	2006 Oct 8
IRAS 09539+0857	1100267.1	2007 May 19
IRAS 10035+2740	1100216.1	2007 May 15
IRAS 10091+4704	1100122.1	2007 May 7
IRAS 10494+4424	1100266.1	2007 May 16
IRAS 10594+3818	1100021.1	2006 Nov 23
IRAS 11028+3130	1100006.1	2006 Nov 26
IRAS 11180+1623	1100202.1	2007 Jun 5
IRAS 11387+4116	1100269.1	2007 May 29
IRAS 12447+3721	1100022.1	2006 Dec 15
IRAS 12540+5708 (Mrk 231)	1100271.1	2007 May 30
IRAS 13428+5608 (Mrk 273)	1100273.1	2007 Jun 8
IRAS 13469+5833	1100023.1	2006 Dec 7
IRAS 13539+2920	1100235.1	2007 Jul 6
IRAS 14121–0126	1100011.1	2007 Jan 22
IRAS 14202+2615	1100212.1	2007 Jul 15
IRAS 14394+5332	1100283.1	2007 Jun 25
IRAS 15043+5754	1100213.1	2007 Jun 23
IRAS 16333+4630	1100013.1	2007 Feb 8
IRAS 16468+5200	1100249.1	2007 Aug 10
IRAS 16487+5447	1100247.1	2007 Aug 6
IRAS 17028+5817	1100248.1	2007 Aug 8
IRAS 17044+6720	1100297.1	2007 May 31
IRAS 17068+4027	1100026.1	2007 Feb 26
IRAS 17179+5444	1100253.1	2007 Aug 23
IRAS 19254–7245	1100132.1	2007 Mar 30
IRAS 21477+0502	1100207.1	2007 May 22
IRAS 22088–1831	1100214.1	2007 May 19
IRAS 23128–5919	1100294.1	2007 May 10
IRAS 23129+2548	1100015.1	2006 Dec 22
IRAS 23498+2423	1100287.1	2007 Jul 1

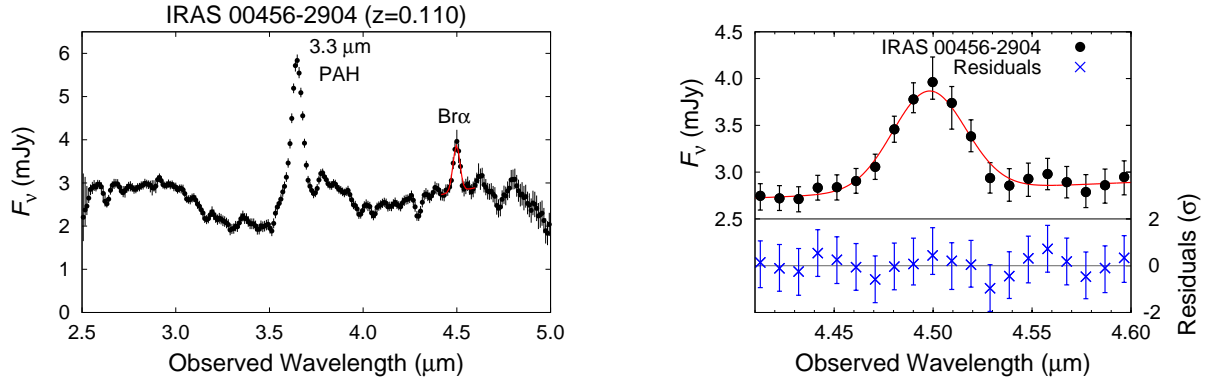


Figure 1. Typical example of the *AKARI* IRC 2.5–5.0 μm spectra of ULIRGs. The left panel presents the entire spectrum, while the right panel shows the magnification around the Br α line of the left panel. The best-fit Gaussian profile for the Br α line is plotted with the red solid line. The residual spectrum of the best-fit is also displayed in the left panel with the blue crosses.

Table 2
Basic Information of Our Target ULIRGs.

Object Name	z^a	D_L^b (Mpc)	F_{25}^c (Jy)	F_{60}^c (Jy)	F_{100}^c (Jy)	L_{IR}^d ($10^{12} L_\odot$)	Optical ^e class	$F_{3.3}^f$ ($10^{-14} \text{ erg s}^{-1} \text{ cm}^{-2}$)	Ref. ^g
IRAS 00183–7111 ^{hi}	0.327	1717	0.13	1.20	1.19	7.56	LINER	< 1.8	1
IRAS 00456–2904	0.110	508	0.14	2.60	3.38	1.40	H II	4.0	2
IRAS 00482–2721	0.129	604	< 0.18	1.13	1.84	1.17	LINER	1.3	3
IRAS 01199–2307	0.156	744	< 0.16	1.61	1.37	1.22	H II	0.8	2
IRAS 01298–0744 ^j	0.136	640	0.19	2.47	2.08	1.62	H II	1.7	4
IRAS 01355–1814 ^j	0.192	935	0.12	1.40	1.74	2.80	H II	0.6	5
IRAS 01494–1845	0.158	753	< 0.15	1.29	1.85	1.71	Unclassified	2.2	5
IRAS 01569–2939	0.140	660	0.14	1.73	1.51	1.26	H II	1.8	3
IRAS 02480–3745	0.165	790	< 0.11	1.25	1.49	1.43	Unclassified	1.5	5
IRAS 03209–0806	0.166	798	< 0.13	1.00	1.69	1.77	H II	2.2	6
IRAS 03521+0028 ^j	0.152	721	0.20	2.52	3.62	3.32	LINER	2.2	7
IRAS 04074–2801 ^j	0.154	731	0.07	1.33	1.72	1.47	LINER	0.9	2
IRAS 04313–1649	0.268	1364	0.07	1.01	1.10	3.58	Unclassified	< 0.4	5
IRAS 05020–2941	0.154	734	0.10	1.93	2.06	1.79	LINER	1.0	2
IRAS 05189–2524 ^k	0.043	187	3.47	13.25	11.84	1.55	Seyfert 2	30.0	8
IRAS 06035–7102 ^{ilm}	0.079	359	0.62	5.34	6.18	1.68	H II	11.2	4
IRAS 08572+3915 ^k	0.058	260	1.76	7.30	4.77	1.37	LINER	< 4.2	9
IRAS 08591+5248	0.157	750	< 0.16	1.01	1.53	1.50	Unclassified	1.4	10
UGC 5101 ^{kn}	0.039	173	1.02	11.68	19.91	1.05	LINER	22.5	11
IRAS 09463+8141	0.156	743	< 0.07	1.43	2.29	1.81	LINER	2.2	5
IRAS 09539+0857	0.129	603	< 0.15	1.44	1.04	0.62	LINER	1.2	12
IRAS 10035+2740	0.166	793	< 0.17	1.14	1.63	1.77	Unclassified	1.4	13
IRAS 10091+4704	0.246	1237	< 0.08	1.18	1.55	3.49	LINER	0.7	5
IRAS 10494+4424	0.092	420	0.16	3.53	5.41	1.48	LINER	3.6	7
IRAS 10594+3818	0.158	753	< 0.15	1.29	1.89	1.74	H II	2.6	5
IRAS 11028+3130 ^j	0.199	971	0.09	1.02	1.44	2.47	LINER	0.6	12
IRAS 11180+1623	0.166	795	< 0.19	1.19	1.60	1.80	LINER	0.5	5
IRAS 11387+4116	0.149	705	< 0.14	1.02	1.51	1.27	H II	1.9	14
IRAS 12447+3721 ^j	0.158	753	0.10	1.04	0.84	1.01	H II	1.3	5
Mrk 231 ^{ik}	0.042	186	8.84	30.80	29.74	3.89	Seyfert 1	76.6	15
Mrk 273 ^{ik}	0.038	166	2.36	22.51	22.53	1.29	Seyfert 2	24.8	7
IRAS 13469+5833 ^j	0.158	752	0.04	1.27	1.73	1.43	H II	1.4	1
IRAS 13539+2920	0.108	500	0.12	1.83	2.73	1.14	H II	4.3	16
IRAS 14121–0126 ^j	0.150	712	0.11	1.39	2.07	1.84	LINER	2.9	3
IRAS 14202+2615	0.159	757	0.15	1.49	1.99	2.19	H II	4.2	12
IRAS 14394+5332	0.105	481	0.35	1.95	2.39	1.40	Seyfert 2	6.2	17
IRAS 15043+5754	0.151	714	0.07	1.02	1.50	1.29	H II	2.0	6
IRAS 16333+4630 ^j	0.191	930	0.06	1.19	2.09	2.84	LINER	2.1	7
IRAS 16468+5200	0.150	711	0.10	1.01	1.04	1.06	LINER	0.6	5
IRAS 16487+5447	0.104	477	0.20	2.88	3.07	1.23	LINER	3.3	9
IRAS 17028+5817	0.106	489	0.10	2.43	3.91	1.42	LINER	3.7	9
(E nucleus)	H II	0.4	...
(W nucleus)	LINER	3.3	...
IRAS 17044+6720	0.135	634	0.36	1.28	0.98	1.71	LINER	2.3	18
IRAS 17068+4027	0.179	865	0.12	1.33	1.41	2.04	H II	2.2	5
IRAS 17179+5444	0.147	696	0.20	1.36	1.91	2.03	Seyfert 2	1.2	5
IRAS 19254–7245 ^{lo}	0.062	275	1.34	5.30	6.70	1.54	Seyfert 2	3.8	4
IRAS 21477+0502 ^j	0.171	822	0.16	1.14	1.46	2.19	LINER	0.6	5
IRAS 22088–1831 ^j	0.170	818	0.07	1.73	1.73	1.75	H II	< 0.2	1
IRAS 23128–5919 ^{ikm}	0.045	197	1.64	10.94	10.68	1.04	H II	32.0	19
IRAS 23129+2548 ^j	0.179	864	0.08	1.81	1.64	1.89	LINER	< 0.4	5
IRAS 23498+2423 ^j	0.212	1045	0.12	1.02	1.45	3.17	Seyfert 2	< 1.9	5

^a Redshift.

^b Luminosity distance calculated from z using our adopted cosmology.

^c $IRAS$ fluxes at 25 μm (F_{25}), 60 μm (F_{60}), and 100 μm (F_{100}). These fluxes are taken from the *IRAS* Faint Source Catalog (Moshir et al. 1992), except for galaxies with additional notes.

^d Total infrared (3–1100 μm) luminosity calculated with $L_{IR} = 4\pi D_L^2 (\xi_1 \nu F_{25} + \xi_2 \nu F_{60} + \xi_3 \nu F_{100})$, $(\xi_1, \xi_2, \xi_3) = (2.403, -0.2454, 1.6381)$ (Dale & Helou 2002). For sources with upper limits, we follow the method described in Imanishi et al. (2008, 2010b). The upper and lower limits on the infrared luminosity are obtained by assuming that the actual flux is equal to the *IRAS* upper limit and zero value, respectively, and the average of these values is adopted as the infrared luminosity. Since the calculation is based on our adopted cosmology, the infrared luminosity of IRAS 09539+0857 is estimated to be lower than that of $10^{12} L_\odot$, however, we treat this object as ULIRG in this paper.

^e Optical classification of galaxies. These classifications are taken from Veilleux et al. (1999), except for galaxies with additional notes.

^f Observed flux of 3.3 μm PAH emission. These fluxes are taken from Imanishi et al. (2008), except for galaxies with additional notes.

^g References of redshift: (1) Fisher et al. (1995); (2) 6dF Galaxy Survey (Jones et al. 2004) Data Release (DR) 3 (Jones et al. 2009); (3) 2dF Galaxy Redshift Survey (Colless et al. 2001) Final DR (Colless et al. 2003); (4) Strauss et al. (1992); (5) Kim & Sanders (1998); (6) Sloan Digital Sky Survey (SDSS; York et al. 2000) DR 1 (Abazajian et al. 2003); (7) Downes et al. (1993); (8) Huchra et al. (1983); (9) Murphy et al. (2001); (10) Hwang et al. (2007); (11) Rothberg & Joseph (2006); (12) Darling & Giovanelli (2006); (13) SDSS DR 6 (Adelman-McCarthy et al. 2008); (14) SDSS DR 4 (Adelman-McCarthy et al. 2006); (15) Carilli et al. (1998); (16) Strauss & Huchra (1988); (17) SDSS DR 3 (Abazajian et al. 2005); (18) Nagar et al. (2003); (19) Lauberts & Valentijn (1989).

^h Optical classification is taken from Armus et al. (1989).

ⁱ 3.3 μm PAH emission flux is taken from Imanishi et al. (2010b).

^j $IRAS$ fluxes are taken from Kim & Sanders (1998).

^k $IRAS$ fluxes are taken from Sanders et al. (2003).

^l $IRAS$ fluxes are taken from Sanders et al. (1995).

^m Optical classification is taken from Duc et al. (1997).

ⁿ Optical classification is taken from Veilleux et al. (1995).

^o Optical classification is taken from Mirabel et al. (1991).

$\pm 0.15 \mu\text{m}$ around the central wavelength of the $\text{Br}\alpha$ line. The obtained central wavelengths of the $\text{Br}\alpha$ lines exhibit small discrepancies from those expected from redshifts. The discrepancy is larger than the fitting error of typically $\sim 10^{-3} \mu\text{m}$ but within the wavelength calibration error of $\sim 10^{-2} \mu\text{m}$ (Ohya et al. 2007). Therefore, we shifted the wavelength of the entire spectrum so that the best-fit central wavelength of the $\text{Br}\alpha$ line matches the redshift. The flux of the $\text{Br}\alpha$ line was then calculated by integrating the best-fit Gaussian profile.

3. RESULTS

In this section, we present a result of the measurement of the $\text{Br}\alpha$ line flux in ULIRGs. We utilize the $\text{Br}\alpha$ line luminosity as an indicator of star formation with investigating the effect of heavy dust extinction on the $\text{Br}\alpha$ line. We also present a result of a comparison of the $\text{Br}\alpha$ line with the total infrared luminosity and the $3.3 \mu\text{m}$ PAH emission.

3.1. Resultant Spectra and $\text{Br}\alpha$ Line Fluxes

Figure 1 presents an example of $2.5\text{--}5.0 \mu\text{m}$ spectra of ULIRGs obtained with *AKARI* IRC. Among the sample of galaxies, one source, IRAS 17028+5817, has two nuclei in the source. Since the eastern (E) and western (W) nuclei of this galaxy are resolved with *AKARI* IRC, the spectra of the two nuclei are separately extracted. Thus, in total, 51 spectra are obtained from the 50 observations (Tab. 1).

Among the 51 spectra, three sources (IRAS 00183–7111, IRAS 04313–1649, and IRAS 10091+4704) have a redshift higher than 0.24 and the $\text{Br}\alpha$ line was not observed within the $2.5\text{--}5.0 \mu\text{m}$ wavelength range by *AKARI*. Moreover, the line fitting was not performed for two other sources (IRAS 21477+0502 and IRAS 23129+2548) because their spectra suffer from spectral overlapping with other objects and we were not able to determine the spatial extension of the targets. We therefore performed the line fitting to 46 objects and detected the $\text{Br}\alpha$ line at the 99% confidence level (2.5σ) in 33 objects. In the remaining 13 objects, we derived 2.5σ upper-limit fluxes of the $\text{Br}\alpha$ line. The measured $\text{Br}\alpha$ line fluxes are summarized in Table 3.

3.2. Effect of Dust Extinction on $\text{Br}\alpha$ Line

In the standard extinction curve (e.g., Draine 2003), dust extinction is lower at longer wavelengths. Thus the $\text{Br}\alpha$ line is less affected by dust extinction owing to its infrared wavelength ($4.05 \mu\text{m}$) than the optical Balmer lines and even the infrared $\text{Pa}\alpha$ and $\text{Br}\gamma$ lines ($\sim 2 \mu\text{m}$) widely observed from the ground. Furthermore, from observations of the Galactic center, Fritz et al. (2011) recently showed that extinction at $4 \mu\text{m}$ was about the same as that at $\sim 7\text{--}8 \mu\text{m}$ ($A_{7.5 \mu\text{m}}/A_{4 \mu\text{m}} \sim 0.8$, where A_λ is extinction in magnitude at a wavelength of λ) and was even lower than that at $\sim 9\text{--}20 \mu\text{m}$ ($A_{12.4 \mu\text{m}}/A_{4 \mu\text{m}} \sim 1.3$). This means that the effect of dust extinction on the $\text{Br}\alpha$ line is compatible with (or even lower than) that on other star formation indicators in the mid-infrared wavelength such as the $7.7 \mu\text{m}$ PAH feature or the $[\text{Ne II}] 12.8 \mu\text{m}$ line widely observed with *Spitzer* (e.g., Veilleux et al. 2009). Thus we conclude that the $\text{Br}\alpha$ line is one of the best tracers of star formation in the near-

to mid-infrared wavelength range. However, especially in ULIRGs, which harbor vast amounts of dust, dust extinction could pose a problem even if we use the $\text{Br}\alpha$ line.

As an indicator of extinction, the optical $\text{H}\alpha/\text{H}\beta$ line ratio is widely used (e.g., Kim et al. 1998). The $\text{H}\alpha/\text{H}\beta$ line ratio taken from literature and the inferred visual extinction in our sample are summarized in Table 3. We assume an intrinsic line ratio for $\text{H}\alpha/\text{H}\beta$ of 2.87 (Osterbrock & Ferland 2006, case B with $T = 10000 \text{ K}$ and low-density limit). For the extinction law, the Milky way dust model of Draine (2003) is used ($A_{\text{H}\alpha} = 0.776A_V$, $A_{\text{H}\beta} = 1.17A_V$, and $A_{\text{Br}\alpha} = 3.56 \times 10^{-2}A_V$). The extinction corrected luminosity of the $\text{Br}\alpha$ line ($L_{\text{Br}\alpha}$) is summarized in Table 4.

The visual extinction derived from the optical $\text{H}\alpha/\text{H}\beta$ line ratio is typically a few mag, and the correction factor for the flux of the $\text{Br}\alpha$ line, $C_{\text{Br}\alpha}$, is at most ~ 1.3 (Table 3). If dust obscuration of starburst in these ULIRGs is so heavy, however, optical observations would trace only the outer region of the obscured starburst, and the visual extinction derived from the $\text{H}\alpha/\text{H}\beta$ line ratio would be regarded as a kind of lower limit. For instance, Genzel et al. (1998) reported visual extinction of $5\text{--}50 \text{ mag}$ in ULIRGs based on the *ISO* mid-infrared spectroscopic observations. Here we discuss the uncertainty arising from such heavy dust obscuration.

With our *AKARI* result, we are able to estimate visual extinction using the $\text{Br}\beta$ line ($n: 6 \rightarrow 4$, $\lambda_{\text{rest}} = 2.63 \mu\text{m}$) observed simultaneously with the $\text{Br}\alpha$ line, although it is difficult to measure the flux of the $\text{Br}\beta$ line because of its faintness. In one source among our sample, IRAS 00456–2904 (Figure 1), we marginally detect the $\text{Br}\beta$ line and measure its flux to be $(2.3 \pm 1.0) \times 10^{-15} \text{ erg cm}^{-2} \text{ s}^{-2}$. This yields the $\text{Br}\beta/\text{Br}\alpha$ line ratio of 0.31 ± 0.15 . Adopting an intrinsic line ratio for $\text{Br}\beta/\text{Br}\alpha$ of 0.57 (Osterbrock & Ferland 2006) and $A_{\text{Br}\beta} = 8.09 \times 10^{-2}A_V$ (Draine 2003), we derive visual extinction of $14 \pm 11 \text{ mag}$ from the $\text{Br}\beta/\text{Br}\alpha$ line ratio. This corresponds to a correction factor for the flux of the $\text{Br}\alpha$ line of 1.6 ± 0.5 . Thus, in this source, extinction heavier than that derived from the $\text{H}\alpha/\text{H}\beta$ line ratio ($A_V = 2.17 \pm 0.14 \text{ mag}$) is indicated.

To investigate the effect of heavy dust extinction with the entire sample, we focus on the optical depth of the $9.7 \mu\text{m}$ silicate absorption feature ($\tau_{9.7}$) derived from the *Spitzer* observations. Owing to the mid-infrared wavelength, the $9.7 \mu\text{m}$ silicate absorption feature can probe dust extinction in heavily obscured regions. Table 5 summarizes $\tau_{9.7}$ taken from the literature (references are also listed therein). We convert $\tau_{9.7}$ to visual extinction $A_V^{9.7}$ using the following relation; $A_V^{9.7} (\text{mag}) = (1.08/0.087)\tau_{9.7}$ (Imanishi et al. 2007). We regard $A_V^{9.7}$ as the most extreme extinction in the sample. The mean value of $A_V^{9.7}$ is $\sim 23 \text{ mag}$ in our sample. This corresponds to the correction factor for the flux of the $\text{Br}\alpha$ line of ~ 2.1 . Thus the effect of heavy dust extinction to the $\text{Br}\alpha$ line flux is about a factor of two even in the extreme cases.

In summary, taking the effect of heavy dust extinction into account, we conclude that the intrinsic $\text{Br}\alpha$ line flux is determined within an uncertainty of a factor of two underestimation. Allowing for this uncertainty, we adopt

Table 3
Observed Br α Line Flux and Correction for Dust Extinction.

Object Name	$F_{\text{Br}\alpha}^{\text{a}}$ ($10^{-15} \text{ erg s}^{-1} \text{ cm}^{-2}$)	$\text{H}\alpha/\text{H}\beta^{\text{b}}$	A_V^{c} (mag)	$C_{\text{Br}\alpha}^{\text{d}}$	Ref. ^e
IRAS 00183–7111	... ^f	2.9 ± 1.0	0.06 ± 0.98	1.002 ± 0.032	1
IRAS 00456–2904	7.32 ± 0.82	6.25 ± 0.31	2.17 ± 0.14	1.074 ± 0.005	2
IRAS 00482–2721	3.53 ± 0.81	9.09 ± 0.45	3.22 ± 0.14	1.111 ± 0.005	2
IRAS 01199–2307	< 4.5	6.67 ± 0.33	2.35 ± 0.14	1.080 ± 0.005	2
IRAS 01298–0744	< 2.2	6.67 ± 0.33	2.35 ± 0.14	1.080 ± 0.005	2
IRAS 01355–1814	< 2.6	6.25 ± 0.31	2.17 ± 0.14	1.074 ± 0.005	2
IRAS 01494–1845	5.04 ± 0.81
IRAS 01569–2939	5.71 ± 0.83	16.67 ± 0.83	4.91 ± 0.14	1.175 ± 0.005	2
IRAS 02480–3745	2.94 ± 0.77
IRAS 03209–0806	5.59 ± 0.87	11.11 ± 0.56	3.78 ± 0.14	1.132 ± 0.005	2
IRAS 03521+0028	2.9 ± 1.2	33.3 ± 8.3	6.85 ± 0.70	1.252 ± 0.023	2
IRAS 04074–2801	< 2.1	9.09 ± 0.45	3.22 ± 0.14	1.111 ± 0.005	2
IRAS 04313–1649	... ^f	16.8 ± 3.5	4.94 ± 0.58	1.176 ± 0.019	3
IRAS 05020–2941	2.08 ± 0.74	6.25 ± 0.31	2.17 ± 0.14	1.074 ± 0.005	2
IRAS 05189–2524	17.4 ± 6.9	8.3 ± 2.1	2.98 ± 0.70	1.103 ± 0.023	2
IRAS 06035–7102	7.1 ± 1.7	13.4 ± 4.4	4.30 ± 0.93	1.151 ± 0.030	4 ^g
IRAS 08572+3915	< 14.9	20.8 ± 1.0	5.52 ± 0.14	1.199 ± 0.005	2 ^h
IRAS 08591+5248	2.61 ± 0.75	6.09 ± 0.88	2.10 ± 0.41	1.071 ± 0.013	5
UGC 5101	< 20.4	17.29 ± 0.95	5.02 ± 0.15	1.179 ± 0.005	5
IRAS 09463+8141	3.00 ± 0.90	25.0 ± 6.3	6.05 ± 0.70	1.219 ± 0.023	2
IRAS 09539+0857	2.11 ± 0.64	10.00 ± 0.50	3.49 ± 0.14	1.121 ± 0.005	2
IRAS 10035+2740	< 2.6	8.5 ± 1.1	3.03 ± 0.35	1.105 ± 0.012	5
IRAS 10091+4704	... ^f	12.50 ± 0.63	4.11 ± 0.14	1.144 ± 0.005	2
IRAS 10494+4424	11.59 ± 0.68	9.09 ± 0.45	3.22 ± 0.14	1.111 ± 0.005	2
IRAS 10594+3818	6.7 ± 1.1	5.88 ± 0.29	2.00 ± 0.14	1.068 ± 0.005	2
IRAS 11028+3130	< 6.7	3.45 ± 0.17	0.51 ± 0.14	1.017 ± 0.005	2
IRAS 11180+1623	< 4.1	10.00 ± 0.50	3.49 ± 0.14	1.121 ± 0.005	2
IRAS 11387+4116	5.16 ± 0.71	12.50 ± 0.63	4.11 ± 0.14	1.144 ± 0.005	2
IRAS 12447+3721	4.73 ± 0.85	5.26 ± 0.26	1.69 ± 0.14	1.057 ± 0.005	2
Mrk 231	< 99.7	5.2 ± 2.2	1.6 ± 1.2	1.055 ± 0.039	6
Mrk 273	38.8 ± 2.3	10.00 ± 0.50	3.49 ± 0.14	1.121 ± 0.005	2
IRAS 13469+5833	5.0 ± 1.2	11.11 ± 0.56	3.78 ± 0.14	1.132 ± 0.005	2
IRAS 13539+2920	12.5 ± 1.6	14.29 ± 0.71	4.48 ± 0.14	1.158 ± 0.005	2
IRAS 14121–0126	3.99 ± 0.87	12.50 ± 0.63	4.11 ± 0.14	1.144 ± 0.005	2
IRAS 14202+2615	7.69 ± 0.90	6.25 ± 0.31	2.17 ± 0.14	1.074 ± 0.005	2
IRAS 14394+5332	7.93 ± 0.76	7.69 ± 0.38	2.75 ± 0.14	1.095 ± 0.005	2
IRAS 15043+5754	1.95 ± 0.50	7.69 ± 0.38	2.75 ± 0.14	1.095 ± 0.005	2
IRAS 16333+4630	4.16 ± 0.92	8.33 ± 0.42	2.98 ± 0.14	1.103 ± 0.005	2
IRAS 16468+5200	< 3.9	9.20 ± 0.35	3.25 ± 0.11	1.113 ± 0.003	2 ^h
IRAS 16487+5447	9.33 ± 0.72	5.00 ± 0.25	1.55 ± 0.14	1.052 ± 0.005	2
IRAS 17028+5817E	2.38 ± 0.74	5.56 ± 0.28	1.84 ± 0.14	1.062 ± 0.005	2
IRAS 17028+5817W	5.15 ± 0.77	14.29 ± 0.71	4.48 ± 0.14	1.158 ± 0.005	2
IRAS 17044+6720	6.7 ± 1.7	7.14 ± 0.36	2.55 ± 0.14	1.087 ± 0.005	2
IRAS 17068+4027	8.79 ± 0.95	12.50 ± 0.63	4.11 ± 0.14	1.144 ± 0.005	2
IRAS 17179+5444	4.0 ± 1.1	10.00 ± 0.50	3.49 ± 0.14	1.121 ± 0.005	2
IRAS 19254–7245	15.7 ± 2.5	9.8 ± 1.6	3.43 ± 0.45	1.119 ± 0.015	1
IRAS 21477+0502	... ⁱ	5.88 ± 0.29	2.00 ± 0.14	1.068 ± 0.005	2
IRAS 22088–1831	< 2.2	4.76 ± 0.24	1.41 ± 0.14	1.047 ± 0.005	2
IRAS 23128–5919	64.2 ± 1.5	7.95 ± 0.80	2.85 ± 0.28	1.098 ± 0.009	4 ^h
IRAS 23129+2548	... ⁱ	12.50 ± 0.63	4.11 ± 0.14	1.144 ± 0.005	2
IRAS 23498+2423	< 3.3	7.14 ± 0.36	2.55 ± 0.14	1.087 ± 0.005	2

^a Observed Br α line flux obtained with our *AKARI* result.

^b Flux ratio of H α and H β lines taken from literatures.

^c Visual extinction derived from H α /H β line ratio.

^d Dust-extinction correction factor for Br α line flux.

^e References of optical line fluxes: (1) Buchanan et al. (2006); (2) Veilleux et al. (1999); (3) Rupke et al. (2008); (4) Duc et al. (1997); (5) Hou et al. (2009); (6) Lipari et al. (1994).

^f Redshift is larger than 0.24 and Br α line is not observed within 2.5–5.0 μm wavelength range.

^g Value of W nucleus.

^h Sum of two nuclei.

ⁱ Spectrum suffered from source overlapping.

Table 4
Luminosity of Br α Lines.

Object Name	$L_{\text{Br}\alpha}^{\text{a}}$ ($10^7 L_{\odot}$)	$L_{\text{Br}\alpha}/L_{\text{IR}}$ (10^{-5})
IRAS 00183–7111
IRAS 00456–2904	6.32 ± 0.71	4.50 ± 0.51
IRAS 00482–2721	4.5 ± 1.0	3.83 ± 0.88
IRAS 01199–2307	< 8.4	< 6.9
IRAS 01298–0744	< 3.1	< 1.9
IRAS 01355–1814	< 7.7	< 2.7
IRAS 01494–1845	8.9 ± 1.4	5.21 ± 0.84
IRAS 01569–2939	9.1 ± 1.3	7.2 ± 1.1
IRAS 02480–3745	5.7 ± 1.5	4.0 ± 1.0
IRAS 03209–0806	12.6 ± 2.0	7.1 ± 1.1
IRAS 03521+0028	5.9 ± 2.4	1.78 ± 0.71
IRAS 04074–2801	< 3.9	< 2.6
IRAS 04313–1649
IRAS 05020–2941	3.8 ± 1.3	2.10 ± 0.75
IRAS 05189–2524	2.10 ± 0.84	1.35 ± 0.54
IRAS 06035–7102	3.28 ± 0.78	1.96 ± 0.47
IRAS 08572+3915	< 3.7	< 2.7
IRAS 08591+5248	4.9 ± 1.4	3.26 ± 0.94
UGC 5101	< 2.2	< 2.1
IRAS 09463+8141	6.3 ± 1.9	3.5 ± 1.0
IRAS 09539+0857	2.68 ± 0.81	4.3 ± 1.3
IRAS 10035+2740	< 5.7	< 3.2
IRAS 10091+4704
IRAS 10494+4424	7.08 ± 0.42	4.80 ± 0.28
IRAS 10594+3818	12.6 ± 2.1	7.2 ± 1.2
IRAS 11028+3130	< 20.0	< 8.1
IRAS 11180+1623	< 9.0	< 5.0
IRAS 11387+4116	9.1 ± 1.3	7.22 ± 0.99
IRAS 12447+3721	8.8 ± 1.6	8.7 ± 1.6
Mrk 231	< 11.3	< 2.9
Mrk 273	3.72 ± 0.22	2.88 ± 0.17
IRAS 13469+5833	10.0 ± 2.3	7.0 ± 1.6
IRAS 13539+2920	11.3 ± 1.4	9.9 ± 1.2
IRAS 14121–0126	7.2 ± 1.6	3.93 ± 0.86
IRAS 14202+2615	14.8 ± 1.7	6.73 ± 0.79
IRAS 14394+5332	6.26 ± 0.60	4.47 ± 0.43
IRAS 15043+5754	3.40 ± 0.87	2.63 ± 0.67
IRAS 16333+4630	12.4 ± 2.7	4.35 ± 0.97
IRAS 16468+5200	< 6.8	< 6.4
IRAS 16487+5447	6.97 ± 0.54	5.67 ± 0.44
IRAS 17028+5817	6.32 ± 0.88	4.45 ± 0.62
(E nucleus)	1.88 ± 0.59	...
(W nucleus)	4.44 ± 0.66	...
IRAS 17044+6720	9.1 ± 2.3	5.3 ± 1.4
IRAS 17068+4027	23.4 ± 2.5	11.5 ± 1.2
IRAS 17179+5444	6.8 ± 1.9	3.34 ± 0.92
IRAS 19254–7245	4.16 ± 0.66	2.71 ± 0.43
IRAS 21477+0502
IRAS 22088–1831	< 4.8	< 2.7
IRAS 23128–5919	8.49 ± 0.22	8.17 ± 0.21
IRAS 23129+2548
IRAS 23498+2423	< 12.1	< 3.8

^a Luminosity of the Br α line ($L_{\text{Br}\alpha}$). Dust extinction is corrected with the H α /H β line ratio.

and apply the dust extinction correction estimated from the H α /H β line ratio to the Br α line flux as the minimum correction because the H α /H β line ratio is available for all our targets. At least half of ionizing photons originate from dust obscured regions are expected to be traced by the Br α line, and thus we utilize the Br α line luminosity as a good indicator of star formation.

3.3. Comparison to Other Star-Formation Indicators

The total infrared luminosity is widely used as an indicator of star formation in star-forming galaxies where AGN do not contaminate the luminosity (e.g., Kennicutt & Evans 2012). Thus we expect that $L_{\text{Br}\alpha}$ is correlated

with L_{IR} if L_{IR} is solely governed by star formation. Here we compare $L_{\text{Br}\alpha}$ with L_{IR} .

The left panel of Figure 2 shows the comparison of $L_{\text{Br}\alpha}$ with L_{IR} for the 33 objects in which the Br α line is detected. We find that the galaxies do not follow a single relation and show a scatter in this plot. The correlation coefficient between L_{IR} and $L_{\text{Br}\alpha}$ is calculated to be 0.116, which yields the probability to obtain such a correlation coefficient by chance of 52.6%. This indicates no significant correlation between them.

Within the spectral window of our *AKARI* observation, the 3.3 μm PAH emission, which traces UV photons from OB stars and is also expected to be used as an indicator of star formation, is observed simultaneously with the Br α line. Although complex emission mechanisms make it difficult to quantitatively connect the 3.3 μm PAH emission luminosity ($L_{3.3}$) with the number of ionizing photons, we also expect a correlation between $L_{3.3}$ and $L_{\text{Br}\alpha}$.

The left panel of Figure 3 shows the relation between $L_{3.3}$ and $L_{\text{Br}\alpha}$. We use $L_{3.3}$ listed in Table 5. Dust extinction is corrected for $L_{3.3}$ using the H α /H β line ratio. Extinction at the wavelength of the 3.3 μm PAH emission is assumed to $A_{3.3} = 5.32 \times 10^{-2} A_V$ (Draine 2003). In contrast to the comparison of $L_{\text{Br}\alpha}$ with L_{IR} , $L_{3.3}$ and $L_{\text{Br}\alpha}$ are well correlated with each other, regardless of the optical classifications of the galaxies. The correlation coefficient between $L_{3.3}$ and $L_{\text{Br}\alpha}$ is calculated to be 0.659 for a sample size of 33. The probability of obtaining such a correlation coefficient by chance is less than 10^{-4} . We regard this correlation as statistically significant. We also examine the comparison of fluxes, $F_{3.3}$ and $F_{\text{Br}\alpha}$, in the right panel of Figure 3 to investigate a possible correlation introduced by redshift in the luminosity comparison. The correlation coefficient between $F_{3.3}$ and $F_{\text{Br}\alpha}$ is 0.917, and the probability of obtaining this value by chance is well below 10^{-4} . Thus we conclude that the correlation between the 3.3 μm PAH emission and the Br α line is not affected by redshift and is real.

The result of the correlation between $L_{3.3}$ and $L_{\text{Br}\alpha}$ indicates that they trace the same excitation sources, i.e., star formation. If the broad line region of AGN contributes to line fluxes, hydrogen lines would have a FWHM of a few thousands km s^{-1} (Osterbrock & Ferland 2006). However, the width of the Br α line is consistent with the spectral resolution ($\Delta v \sim 3000 \text{ km s}^{-1}$) in all targets within a fitting uncertainty of $\lesssim 100 \text{ km s}^{-1}$. This indicates that none of the objects show a broad component of the Br α line with a FWHM broader than $\sim 1000 \text{ km s}^{-1}$. Combining the absence of the broad component of the Br α line and the correlation between $L_{\text{Br}\alpha}$ and $L_{3.3}$, we assume that the Br α line and the 3.3 μm PAH emission are entirely produced by star formation. The absence of a correlation between $L_{\text{Br}\alpha}$ and L_{IR} then indicates that L_{IR} has a contribution from energy sources other than star formation, i.e., AGN, in our sample. Thus we conclude that we are able to investigate the contribution of starburst as the dust-enshrouded energy source in ULIRGs with comparing $L_{\text{Br}\alpha}$ with L_{IR} .

The 3.3 μm PAH emission, which is stronger than the Br α line, is detected in almost all our targets, even in the objects in which the Br α line is not observed (Tab. 2). Therefore, we calibrate $L_{3.3}$ with $L_{\text{Br}\alpha}$ to quantitatively

Table 5
Luminosity of 3.3 μm PAH Emission and 9.7 μm Silicate Absorption.

Object Name	$\tau_{9.7}^{\text{a}}$	$A_V^{9.7\text{b}}$ (mag)	$L_{3.3}^{\text{c}}$ ($10^8 L_\odot$)	$L_{3.3}/L_{\text{IR}}$ (10^{-4})	Ref. ^d
IRAS 00183–7111	3.1 ± 0.16	38.5 ± 1.9	< 16.6	< 2.19	1
IRAS 00456–2904	1.2 ± 0.12	14.9 ± 1.5	3.6 ± 1.1	2.55 ± 0.77	2
IRAS 00482–2721	2.1 ± 0.11	26.1 ± 1.3	1.73 ± 0.52	1.49 ± 0.45	2
IRAS 01199–2307	2.4 ± 0.12	29.8 ± 1.5	1.55 ± 0.46	1.27 ± 0.38	3
IRAS 01298–0744	4.0 ± 0.20	49.7 ± 2.5	2.44 ± 0.73	1.51 ± 0.45	2
IRAS 01355–1814	2.4 ± 0.12	29.8 ± 1.5	1.82 ± 0.55	0.65 ± 0.19	3
IRAS 01494–1845	1.6 ± 0.16	19.9 ± 2.0	3.9 ± 1.2	2.28 ± 0.68	3
IRAS 01569–2939	2.8 ± 0.14	34.8 ± 1.7	3.11 ± 0.93	2.46 ± 0.74	2
IRAS 02480–3745	1.4 ± 0.14	17.4 ± 1.7	2.92 ± 0.88	2.04 ± 0.61	4
IRAS 03209–0806	1.0 ± 0.10	12.4 ± 1.2	5.3 ± 1.6	2.96 ± 0.89	4
IRAS 03521+0028	1.3 ± 0.13	16.1 ± 1.6	5.0 ± 1.5	1.50 ± 0.45	3
IRAS 04074–2801	3.0 ± 0.15	37.3 ± 1.9	1.75 ± 0.53	1.19 ± 0.36	4
IRAS 04313–1649	2.8 ± 0.14	34.8 ± 1.7	< 3.0	< 0.82	3
IRAS 05020–2941	2.4 ± 0.12	29.8 ± 1.5	1.87 ± 0.56	1.05 ± 0.31	4
IRAS 05189–2524	0.3 ± 0.02	3.92 ± 0.21	3.8 ± 1.1	2.45 ± 0.74	5
IRAS 06035–7102	2.9 ± 0.15	36.0 ± 1.8	5.6 ± 1.7	3.3 ± 1.0	1
IRAS 08572+3915	3.8 ± 0.19	47.2 ± 2.4	< 1.2	< 0.84	2
IRAS 08591+5248	1.0 ± 0.10	12.4 ± 1.2	2.72 ± 0.82	1.81 ± 0.54	4
UGC 5101	1.6 ± 0.08	20.1 ± 1.0	2.68 ± 0.80	2.55 ± 0.77	5
IRAS 09463+8141	2.0 ± 0.20	24.8 ± 2.5	5.1 ± 1.5	2.82 ± 0.85	2
IRAS 09539+0857	3.5 ± 0.18	43.5 ± 2.1	1.61 ± 0.48	2.59 ± 0.78	2
IRAS 10035+2740	2.0 ± 0.20	24.8 ± 2.5	3.18 ± 0.96	1.79 ± 0.54	3
IRAS 10091+4704	2.5 ± 0.13	31.0 ± 1.6	4.1 ± 1.2	1.17 ± 0.35	3
IRAS 10494+4424	1.7 ± 0.17	21.1 ± 2.1	2.32 ± 0.70	1.57 ± 0.47	2
IRAS 10594+3818	1.0 ± 0.10	12.4 ± 1.2	5.1 ± 1.5	2.91 ± 0.87	4
IRAS 11028+3130	2.5 ± 0.13	31.0 ± 1.6	1.81 ± 0.54	0.73 ± 0.22	3
IRAS 11180+1623	2.0 ± 0.20	24.8 ± 2.5	1.17 ± 0.35	0.65 ± 0.19	3
IRAS 11387+4116	1.1 ± 0.11	13.7 ± 1.4	3.6 ± 1.1	2.84 ± 0.85	2
IRAS 12447+3721	1.7 ± 0.17	21.1 ± 2.1	2.50 ± 0.75	2.46 ± 0.74	4
Mrk 231	0.6 ± 0.03	7.98 ± 0.43	8.9 ± 2.7	2.29 ± 0.70	5
Mrk 273	1.7 ± 0.09	21.7 ± 1.1	2.52 ± 0.76	1.95 ± 0.58	5
IRAS 13469+5833	1.7 ± 0.17	21.1 ± 2.1	2.97 ± 0.89	2.08 ± 0.62	3
IRAS 13539+2920	1.6 ± 0.16	19.9 ± 2.0	4.2 ± 1.3	3.7 ± 1.1	2
IRAS 14121–0126	1.3 ± 0.13	16.1 ± 1.6	5.6 ± 1.7	3.05 ± 0.92	4
IRAS 14202+2615	0.7 ± 0.07	8.69 ± 0.86	8.3 ± 2.5	3.8 ± 1.1	4
IRAS 14394+5332	5.1 ± 1.5	3.7 ± 1.1	...
IRAS 15043+5754	1.4 ± 0.14	17.4 ± 1.7	3.6 ± 1.1	2.81 ± 0.84	4
IRAS 16333+4630	1.3 ± 0.13	16.1 ± 1.6	6.5 ± 2.0	2.31 ± 0.69	3
IRAS 16468+5200	2.5 ± 0.13	31.0 ± 1.6	1.11 ± 0.33	1.04 ± 0.31	2
IRAS 16487+5447	1.8 ± 0.18	22.4 ± 2.2	2.53 ± 0.76	2.06 ± 0.62	2
IRAS 17028+5817	1.5 ± 0.15	18.6 ± 1.9	3.38 ± 0.92	2.38 ± 0.65	2
(E Nucleus)	0.33 ± 0.10
(W Nucleus)	3.06 ± 0.92
IRAS 17044+6720	1.8 ± 0.18	22.4 ± 2.2	3.26 ± 0.98	1.91 ± 0.57	2
IRAS 17068+4027	1.8 ± 0.18	22.4 ± 2.2	6.3 ± 1.9	3.07 ± 0.92	3
IRAS 17179+5444	2.15 ± 0.64	1.06 ± 0.32	...
IRAS 19254–7245	1.3 ± 0.07	16.7 ± 0.9	1.06 ± 0.32	0.69 ± 0.21	5
IRAS 21477+0502	0.8 ± 0.08	9.9 ± 1.0	1.39 ± 0.42	0.64 ± 0.19	4
IRAS 22088–1831	2.6 ± 0.13	32.3 ± 1.6	< 0.45	< 0.26	4
IRAS 23128–5919	4.4 ± 1.3	4.3 ± 1.3	...
IRAS 23129+2548	2.6 ± 0.13	32.3 ± 1.6	< 1.1	< 0.60	3
IRAS 23498+2423	0.6 ± 0.03	7.48 ± 0.36	< 7.3	< 2.3	6

^a Optical depth of the 9.7 μm silicate absorption.

^b Visual extinction derived from $\tau_{9.7}$.

^c Luminosity of the 3.3 μm PAH emission. Dust extinction is corrected using the $\text{H}\alpha/\text{H}\beta$ ratio.

^d References of $\tau_{9.7}$: (1) Dartois & Muñoz-Caro (2007); (2) Imanishi et al. (2007); (3) Imanishi (2009); (4) Imanishi et al. (2010a); (5) Wu et al. (2009); (6) Willett et al. (2011).

investigate star formation in the objects with no $\text{Br}\alpha$ line detection. From the correlation between $L_{3.3}$ with $L_{\text{Br}\alpha}$, we assume a proportionality between them. The mean $L_{\text{Br}\alpha}/L_{3.3}$ ratio is calculated as

$$L_{\text{Br}\alpha}/L_{3.3} = 0.177 \pm 0.003. \quad (1)$$

This relation quantitatively associates $L_{3.3}$ with the number of ionizing photons from OB stars. Thus we

utilize $L_{3.3}$ as a quantitative indicator of star formation for galaxies in which the $\text{Br}\alpha$ line is not detected.

When using the 3.3 μm PAH emission as a proxy of star formation, Kim et al. (2012) pointed out a caveat that $L_{3.3}/L_{\text{IR}}$ decreases as L_{IR} increases within an infrared luminosity range of $10^{10} L_\odot < L_{\text{IR}} < 10^{13} L_\odot$, and thus, the power of $L_{3.3}$ as an indicator of star formation may be hampered in ULIRGs. This deficit of $L_{3.3}$ was found

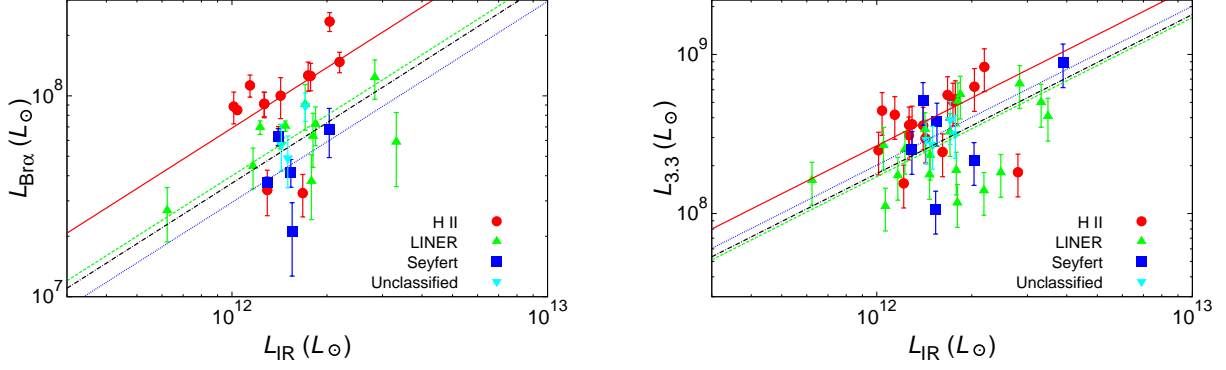


Figure 2. Comparison of the Br α line luminosity ($L_{\text{Br}\alpha}$; left) and the 3.3 μm PAH emission luminosity ($L_{3.3}$; right) with the total infrared luminosity (L_{IR}). The symbols and colors represent the optical classifications of the galaxy. The red solid, green dashed, blue dotted, and black dashed-dotted lines indicate the mean $L_{\text{Br}\alpha}/L_{\text{IR}}$ ($L_{3.3}/L_{\text{IR}}$) ratio for H II galaxies, LINERs, Seyferts, and the combination of LINERs and Seyferts, respectively.

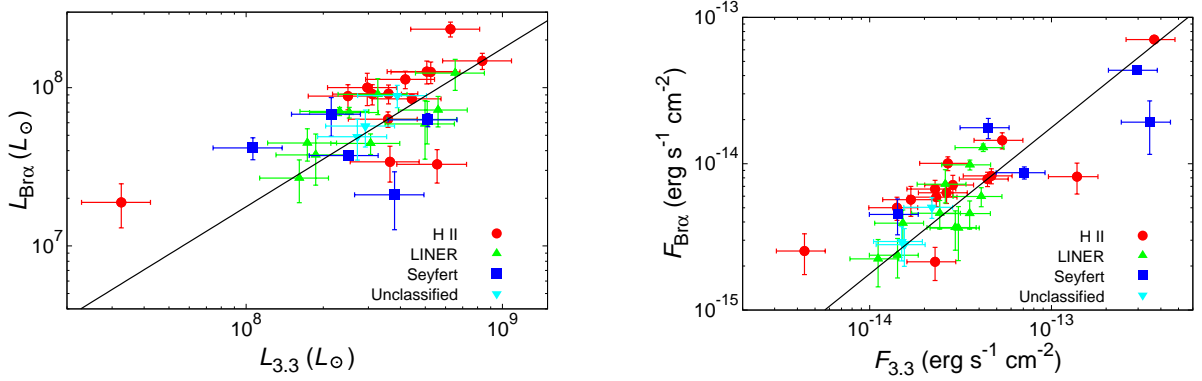


Figure 3. Comparison of the Br α line with the 3.3 μm PAH emission. The left panel shows the comparison of the luminosities, while the right panel presents the comparison of the fluxes. The symbols and colors represent the optical classifications of the galaxy. The solid line shows the mean $L_{\text{Br}\alpha}/L_{3.3}$ ($F_{\text{Br}\alpha}/F_{3.3}$) ratio of 0.177 ± 0.003 .

even if the sources likely to be contaminated by AGN activity are excluded (Yamada et al. 2013). However, we obtain a clear correlation between $L_{3.3}$ and $L_{\text{Br}\alpha}$. We attribute this result to the narrowness of the infrared luminosity range of our sample (most of them lie within $10^{12} L_{\odot} < L_{\text{IR}} < 10^{12.5} L_{\odot}$). The infrared luminosity of the objects where the Br α line is not detected is also in this luminosity range, and hence, we assume that the proportionality of Equation (1) is also valid for these objects.

The right panel of Figure 2 shows the comparison of $L_{3.3}$ with L_{IR} . The number of the sample is increased from 33 in the left panel of the comparison of $L_{\text{Br}\alpha}$ with L_{IR} to 46 with the use of the 3.3 μm PAH emission. In this larger sample, we again find that galaxies show a significant scatter. The correlation coefficient between L_{IR} and $L_{3.3}$ is calculated to be 0.161, yielding the probability of obtaining such a correlation coefficient by chance of 29.7%. The correlation between L_{IR} and $L_{\text{Br}\alpha}$ is not significant, as well as that between L_{IR} and $L_{3.3}$. We discuss the origin of these scatters in the next section.

4. DISCUSSION

In §3, we utilize the luminosities of the Br α line and the 3.3 μm PAH emission as indicators of star formation. Using these indicators, we discuss the contribution of

starburst to the total energy from ULIRGs.

4.1. Starburst Contribution

The optical classifications of ULIRGs are mainly based on the optical emission line ratios (Baldwin et al. 1981) and reflect a qualitative difference of the energy sources, while they have little quantitative information. We investigate the fractional contribution of starburst to the total infrared luminosity with the $L_{\text{Br}\alpha}/L_{\text{IR}}$ and $L_{3.3}/L_{\text{IR}}$ ratios and discuss the quantitative difference of the energy sources among the galaxies with different optical classifications.

4.1.1. Difference among Galaxies with Different Optical Classifications

Focusing on the optical classifications of the galaxies, we find a trend that the galaxies classified as LINERs or Seyferts are distributed lower than those classified as H II galaxies in both the panels of Figure 2. This indicates that LINERs and Seyferts have lower $L_{\text{Br}\alpha}/L_{\text{IR}}$ and $L_{3.3}/L_{\text{IR}}$ ratios than H II galaxies. Here we discuss the significance of these differences.

The left panel of Figure 4 compares a distribution of the $L_{\text{Br}\alpha}/L_{\text{IR}}$ ratio for H II galaxies, LINERs, and Seyferts. The distributions of LINERs and Seyferts are similar with each other, while that of H II galaxies clearly

deviates from the others. To investigate whether the difference of the $L_{\text{Br}\alpha}/L_{\text{IR}}$ ratio is statistically significant, we performed the Kolmogorov–Smirnov (K–S) test between the galaxies with the different optical classifications. The K–S test probabilities that the two sets of samples originate from the same population are summarized in Table 6. The K–S probability between LINERs and Seyferts is 8.5×10^{-2} and indicates no significant difference between them. On the other hand, H II galaxies show a probability of less than 5×10^{-3} against LINERs or Seyferts. If we combine LINERs and Seyferts, the probability that H II galaxies and the others are drawn from the same population is 1.4×10^{-4} . This difference is statistically significant, and we conclude that the $L_{\text{Br}\alpha}/L_{\text{IR}}$ ratio is statistically different between H II galaxies and LINERs/Seyferts.

The right panel of Figure 4 is the same as the left panel, but for the $L_{3.3}/L_{\text{IR}}$ ratio with the larger sample. The distribution of H II galaxies again deviates from the two other classifications. We performed the K–S test for the $L_{3.3}/L_{\text{IR}}$ ratio in the same way as the $L_{\text{Br}\alpha}/L_{\text{IR}}$ ratio and summarize the K–S probabilities for the $L_{3.3}/L_{\text{IR}}$ ratio in Table 6. The K–S test between LINERs and Seyferts again indicates no significant difference between them, while the probability between H II galaxies and the combination of LINERs and Seyferts is 4.0×10^{-3} . This means that the distribution of the $L_{3.3}/L_{\text{IR}}$ is statistically different between H II galaxies and LINERs/Seyferts. Thus the result we obtained with the $L_{\text{Br}\alpha}/L_{\text{IR}}$ ratio is reproduced using $L_{3.3}$ with the larger sample.

The mean $L_{\text{Br}\alpha}/L_{\text{IR}}$ ratio in each classification is calculated and shown in Table 7. The combination of LINERs and Seyferts yields the mean $L_{\text{Br}\alpha}/L_{\text{IR}}$ ratio of 3.7×10^{-5} , which is about half of that in H II galaxies (6.9×10^{-5}). To investigate whether the mean $L_{\text{Br}\alpha}/L_{\text{IR}}$ ratio in LINERs or Seyferts is statistically lower than that in H II galaxies, we performed the Student’s t test. The t -test probabilities that two sets of samples originate from populations with the same mean $L_{\text{Br}\alpha}/L_{\text{IR}}$ ratio are summarized in Table 6. The test between LINERs and Seyferts indicates that there is no significant difference between them, whereas H II galaxies show a low probability against the others. The probability between H II galaxies and the combination of LINERs and Seyferts is 9.0×10^{-4} , which is statistically significant. Thus, we conclude that the mean $L_{\text{Br}\alpha}/L_{\text{IR}}$ ratio in LINERs and Seyferts is significantly lower, about half of that in H II galaxies.

In the same way as the $L_{\text{Br}\alpha}/L_{\text{IR}}$ ratio, the difference of the mean $L_{3.3}/L_{\text{IR}}$ ratio (Table 7) between the galaxies with different optical classifications is examined with the Student’s t test. The result is summarized in Table 6. From the t test probabilities for the $L_{3.3}/L_{\text{IR}}$ ratio, we conclude that the mean $L_{3.3}/L_{\text{IR}}$ ratio in LINERs and Seyferts is significantly lower than that in H II galaxies. This is consistent with the result obtained from the $L_{\text{Br}\alpha}/L_{\text{IR}}$ ratio. Thus, with the larger sample, the difference among the galaxies with different optical classifications is further confirmed.

We here discuss the possible effect of dust extinction to the difference of the $L_{\text{Br}\alpha}/L_{\text{IR}}$ and $L_{3.3}/L_{\text{IR}}$ ratios. To explain the difference of the mean $L_{\text{Br}\alpha}/L_{\text{IR}}$ or $L_{3.3}/L_{\text{IR}}$

ratio among the galaxies with different optical classifications with dust extinction, extinction should be much higher in LINERs and Seyferts than in H II galaxies. However, Veilleux et al. (2009) reported that the optical depth of the $9.7 \mu\text{m}$ silicate absorption was generally smaller in Seyferts than in H II galaxies based on the *Spitzer* results. This indicates that the dust extinction in H II galaxies is generally higher than that in Seyferts and is opposite to the above scenario. Therefore, we conclude that the difference of the mean $L_{\text{Br}\alpha}/L_{\text{IR}}$ and $L_{3.3}/L_{\text{IR}}$ ratios among the galaxies with different optical classifications cannot be explained by the effect of heavy dust extinction.

In summary, we conclude that the mean $L_{\text{Br}\alpha}/L_{\text{IR}}$ and $L_{3.3}/L_{\text{IR}}$ ratios are significantly lower in LINERs and Seyferts than in H II galaxies. This difference is not attributable to the effect of dust extinction.

4.1.2. Fractional Contribution of Starburst as Energy Sources

We propose that the $L_{\text{Br}\alpha}/L_{\text{IR}}$ and $L_{3.3}/L_{\text{IR}}$ ratios reflect the fractional contribution of starburst to the total infrared luminosity, and the relative difference of the ratios among the galaxies with the different optical classifications shows the difference of the energy sources of them.

We here assume that H II galaxies are completely energized by starburst, and the $L_{\text{Br}\alpha}/L_{\text{IR}}$ ratio of 6.9×10^{-5} , which is the mean ratio in H II galaxies, corresponds to the starburst contribution of 100%. On the basis of this assumption, we estimate the starburst contribution as $R_{\text{SB}}^{\text{AKARI}} = (L_{\text{Br}\alpha}/L_{\text{IR}})/(L_{\text{Br}\alpha}/L_{\text{IR}})_0$, where $(L_{\text{Br}\alpha}/L_{\text{IR}})_0 = 6.9 \times 10^{-5}$.

Even the *AKARI* observations, however, could be affected by dust extinction. To verify this effect, we compare our result with the mid-infrared spectroscopic results obtained by *Spitzer* IRS spectroscopy, which is expected to be less affected by dust extinction. Veilleux et al. (2009) summarized the six independent diagnostics to estimate the starburst/AGN contribution in ULIRGs based on *Spitzer* observations. Among our targets, 11 galaxies are also reported in Veilleux et al. (2009), and the starburst contribution to the bolometric luminosity ($R_{\text{SB}}^{\text{Spitzer}}$) in these galaxies is calculated. To see the consistency of our work and the previous *Spitzer* works, we compare $R_{\text{SB}}^{\text{AKARI}}$ with $R_{\text{SB}}^{\text{Spitzer}}$ in Figure 5.

Figure 5 shows general agreement between $R_{\text{SB}}^{\text{AKARI}}$ and $R_{\text{SB}}^{\text{Spitzer}}$, but we note $R_{\text{SB}}^{\text{Spitzer}}$ might be slightly higher than $R_{\text{SB}}^{\text{AKARI}}$ especially in LINERs. To investigate the difference of $R_{\text{SB}}^{\text{Spitzer}}$ and $R_{\text{SB}}^{\text{AKARI}}$, we estimate the error-weighted mean $R_{\text{SB}}^{\text{Spitzer}}/R_{\text{SB}}^{\text{AKARI}}$ ratio. The ratio of the total sample is 0.84 ± 0.15 , while it is 0.69 ± 0.44 , 1.13 ± 0.15 , and 1.28 ± 0.16 in H II galaxies, Seyferts, and LINERs, respectively. The biggest deviation of the ratio from unity is seen in LINERs with the level of about 30%, but the significance level is not high (1.8σ). Due to the limited number of samples, we cannot deny the possibility that the two results might be different, but the current sample does not show the clear difference between the starburst contributions estimated by the two methods. We hence conclude that our result is consistent with the *Spitzer* result, and so $R_{\text{SB}}^{\text{AKARI}}$ can be used

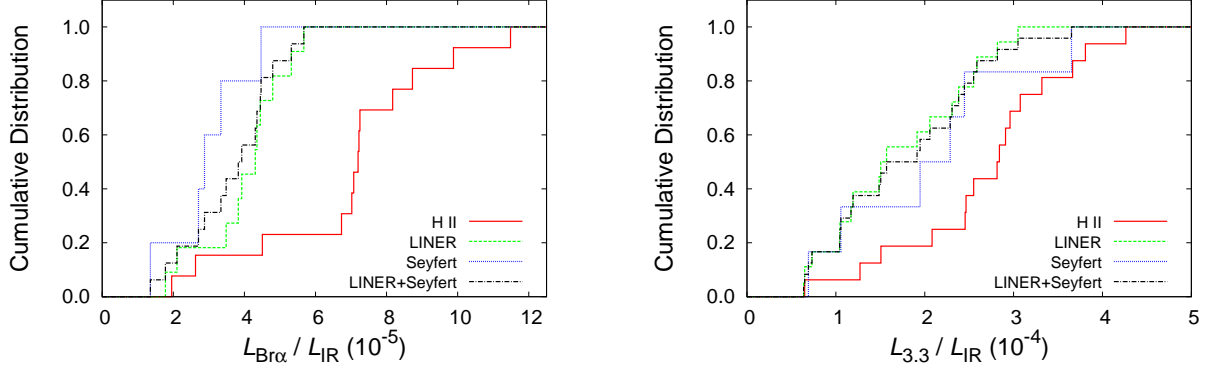


Figure 4. Cumulative distribution for the K-S test of the $L_{\text{Br}\alpha}/L_{\text{IR}}$ ratio (left) and the $L_{3.3}/L_{\text{IR}}$ ratio (right) for H II galaxies (red solid line), LINERs (green dashed line), Seyferts (blue dotted line), and the combination of LINERs and Seyferts (black dashed-dotted line).

Table 6
Statistical Tests for $L_{\text{Br}\alpha}/L_{\text{IR}}$ and $L_{3.3}/L_{\text{IR}}$.

Optical Class	Probability for $L_{\text{Br}\alpha}/L_{\text{IR}}$		Probability for $L_{3.3}/L_{\text{IR}}$	
	Same Population (K-S Test)	Same Mean (t Test)	Same Population (K-S Test)	Same Mean (t Test)
H II vs LINER	6.5×10^{-4}	2.4×10^{-3}	1.1×10^{-2}	2.8×10^{-3}
H II vs Seyfert	4.1×10^{-3}	5.6×10^{-3}	6.2×10^{-2}	1.8×10^{-1}
LINER vs Seyfert	8.5×10^{-2}	1.2×10^{-1}	8.1×10^{-1}	4.5×10^{-1}
H II vs LINER & Seyfert	1.4×10^{-4}	9.0×10^{-4}	4.0×10^{-3}	3.7×10^{-3}

Table 7
Mean and Deviation of $L_{\text{Br}\alpha}/L_{\text{IR}}$ and $L_{3.3}/L_{\text{IR}}$.

Optical Class	$L_{\text{Br}\alpha}/L_{\text{IR}}$			$L_{3.3}/L_{\text{IR}}$		
	Number of Objects	Mean (10^{-5})	Deviation ^a (10^{-5})	Number of Objects	Mean (10^{-4})	Deviation ^a (10^{-4})
H II	13	6.9	2.6	16	2.7	0.9
LINER	11	4.0	1.2	18	1.7	0.8
Seyfert	5	3.0	1.1	6	2.0	1.1
LINER & Seyfert	16	3.7	1.2	24	1.8	0.8

^a 1- σ standard deviation.

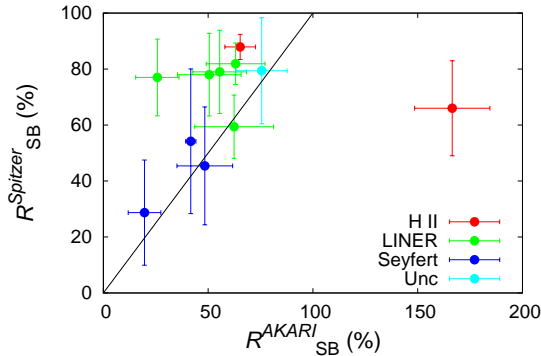


Figure 5. Comparison of the starburst contribution to the bolometric luminosity of the galaxy measured by the *Spitzer* result ($R_{\text{SB}}^{\text{Spitzer}}$) with that estimated from our *AKARI* result ($R_{\text{SB}}^{\text{AKARI}}$; see §4.1.1). $R_{\text{SB}}^{\text{Spitzer}}$ is calculated from Column 8 of Table 12 in Veilleux et al. (2009). The error bar of $R_{\text{SB}}^{\text{Spitzer}}$ represents the standard deviation of the six methods of Table 12 in Veilleux et al. (2009). The symbols and colors represent the optical classifications of the galaxy. The black solid line indicates $R_{\text{SB}}^{\text{Spitzer}} = R_{\text{SB}}^{\text{AKARI}}$.

as a quantitative indicator of the starburst contribution to the total infrared luminosity. We discuss below the energy sources of the galaxies using the $L_{\text{Br}\alpha}/L_{\text{IR}}$ ratio.

We should note that the mean $R_{\text{SB}}^{\text{Spitzer}}/R_{\text{SB}}^{\text{AKARI}}$ ratio in the entire sample is affected by one outlying H II galaxy, IRAS 17068+4027. If we calculate the mean $R_{\text{SB}}^{\text{Spitzer}}/R_{\text{SB}}^{\text{AKARI}}$ ratio without IRAS 17068+4027, the ratio becomes 1.30 ± 0.08 (c.f., 0.84 ± 0.15 with IRAS 17068+4027), and so our *AKARI* observation could underestimate the starburst contribution about 30% relative to the *Spitzer* observation. We have searched possible cause of the high $R_{\text{SB}}^{\text{AKARI}}$ value relative to $R_{\text{SB}}^{\text{Spitzer}}$ in IRAS 17068+4027, but have not successfully identified the cause. For example, we cannot attribute this to the hidden AGN activity, since Figure 5 shows that the $R_{\text{SB}}^{\text{Spitzer}}/R_{\text{SB}}^{\text{AKARI}}$ ratio of Seyferts, which are dominated by AGN, is not deviated from unity. Moreover, we cannot find any clear evidence of the presence of AGN in this galaxy from our observation (e.g., absence of the broad line) and other literature (e.g., Veilleux et al. 1997; Kim et al. 1998). We hence include this

galaxy in the estimate of $R_{\text{SB}}^{\text{Spitzer}}/R_{\text{SB}}^{\text{AKARI}}$ since no clear reason to ignore this galaxy has been found.

4.1.3. Energy Sources of ULIRGs

Starburst is thought to be the dominant energy source in H II galaxies, while AGN are considered to dominate in Seyferts. The result that the mean $L_{\text{Br}\alpha}/L_{\text{IR}}$ ratio is lower in Seyferts than in H II galaxies confirms this difference of energy sources. The mean $L_{\text{Br}\alpha}/L_{\text{IR}}$ ratio in Seyferts is about 43% of that in H II galaxies. This means that the fractional contribution of starburst to the total infrared luminosity in Seyferts is $\sim 43\%$. Given the result that LINERs also have a lower ($\sim 58\%$) $L_{\text{Br}\alpha}/L_{\text{IR}}$ ratio than H II galaxies, energy sources other than starburst are needed in LINERs. The $L_{\text{Br}\alpha}/L_{\text{IR}}$ ratio in LINERs is similar to that in Seyferts, and thus, we propose that AGN are needed as energy generation mechanisms in LINERs, as well as Seyferts. The $L_{3.3}/L_{\text{IR}}$ ratio in LINERs is also similar to that in Seyferts and lower than that in H II galaxies. Thus the idea that AGN are needed in LINERs, as well as Seyferts, is also supported in the larger sample.

The combination of LINERs and Seyferts yields the mean $L_{\text{Br}\alpha}/L_{\text{IR}}$ ratio of 3.7×10^{-5} , which indicates that the fractional contribution of starburst to the total infrared luminosity in these galaxies is $\sim 50\%$. With the larger sample, using the $L_{3.3}/L_{\text{IR}}$ ratio, the contribution of starburst to the total infrared luminosity in the combination of LINERs and Seyferts is estimated as $\sim 67\%$. From this result, it is inferred that AGN produce a significant fraction ($\sim 33\%$) of the total infrared luminosity in LINERs and Seyferts, causing the separation of the ratios between H II galaxies and LINERs/Seyferts. As a whole, our result indicates that AGN account for about one-third of the total infrared luminosity of LINERs and Seyferts, and starburst explains the remaining infrared luminosity of ULIRGs. The mean $L_{3.3}/L_{\text{IR}}$ ratio in the entire sample is calculated as 2.1×10^{-4} , which yields the contribution of starburst to the total infrared luminosity of $\sim 80\%$. Consequently, the AGN contribution to the total infrared luminosity in the entire sample is indicated as $\sim 20\%$. Thus, we conclude that starburst is the dominant power source for the extreme infrared luminosity of ULIRGs.

In addition to Veilleux et al. (2009), numerous works have been done using the mid-infrared spectroscopy with the *Spitzer* satellite to reveal the dust-enshrouded energy sources of ULIRGs. Armus et al. (2007) investigated the mid-infrared spectra of 10 ULIRGs and found evidence for AGNs in galaxies with optical Seyfert or LINER classifications, while they did not find evidence for buried AGNs in ULIRGs classified optically as H II galaxies. Nardini et al. (2009) analyzed 5–8 μm spectra of 71 ULIRGs and derived AGN/starburst contribution to the overall energy output of each source using the spectral decomposition technique. They found that the main fraction of ULIRG luminosity arose from starburst, while the AGN contribution was non-negligible ($\sim 23\%$). From radio observations of 7 ULIRGs, Prouton et al. (2004) concluded that the AGN contribution was at most 50%. Our conclusion that starburst is the dominant power source for ULIRGs is consistent with these results of the works at the longer wavelength. In particular, our estimation of the AGN contribution to the total

infrared luminosity in our entire sample ($\sim 20\%$) shows a good agreement with the result obtained by Nardini et al. (2009).

As for the less luminous population, luminous infrared galaxies (LIRGs; $L_{\text{IR}} = 10^{11}\text{--}10^{12}L_{\odot}$), Alonso-Herrero et al. (2012) decomposed the *Spitzer* spectra of 53 LIRGs into AGN and starburst components. They found that the AGN contribution was only 5% on average in their sample and the bulk of the infrared luminosity of these LIRGs was due to the starburst activity. Our estimation of the AGN contribution in ULIRGs is larger than this result of the LIRGs observation. As discussed in Alonso-Herrero et al. (2012), this supports the idea that the AGN contribution to the total infrared luminosity increases with the total infrared luminosity. Shipley et al. (2013) investigated mid-infrared PAH emissions in 65 LIRGs and estimated the AGN contribution to the total infrared luminosity in their targets. They divided their sample into a subsample of galaxies with *Spitzer* 3.6–8.0 μm colors indicative of warm dust heated by AGN (IRAGN; 14 galaxies) and those galaxies whose colors indicated starburst processes (non-IRAGN; 65 galaxies). They found that for most IRAGN starburst accounted for 10%–50% of the total IR luminosity, while non-IRAGN were mostly dominated by starburst. Their estimation of the starburst contribution in IRAGN is quite low. It is even lower than our estimation of the starburst contribution in LINERs and Seyferts ($\sim 67\%$). We attribute the low starburst contribution of IRAGN relative to our estimation to the difference of the classification methods of galaxies. We propose that the *Spitzer* classification method of IRAGN separated AGN dominated galaxies better than the optical classification method, which should suffer from the effect of dust extinction, and caused the low starburst contribution in IRAGN sample.

The longer wavelength results rely on a little complicated indicators such as fine structure lines or spectral decomposition techniques which assume empirical starburst and AGN templates. On the other hand, our method is based on the direct indicator of the ionizing photons, the Br α line, and so is able to estimate the contribution of starburst in a robust way. We conclude that the contribution of starburst to the total infrared luminosity is different among the galaxies with different optical classifications. The starburst contribution is estimated as $\sim 67\%$ in LINERs and Seyferts. Our result is consistent with the previous works at the longer wavelength.

4.2. Deficit of Ionizing Photons

Here we revisit the assumption of 100% contribution of starburst in H II galaxies with converting the observed luminosities to the number of ionizing photons. The Br α line luminosity can be converted into the number of ionizing photons, $Q_{\text{Br}\alpha}$, on the assumption of the case B with $T = 10000$ K and low-density limit of the model by Osterbrock & Ferland (2006);

$$Q_{\text{Br}\alpha} \text{ (s}^{-1}\text{)} = 2.54 \times 10^{13} L_{\text{Br}\alpha} \text{ (erg s}^{-1}\text{)}. \quad (2)$$

The number of ionizing photons from OB stars is theoretically related to SFR on the assumption of the initial mass function (e.g., Kennicutt & Evans 2012). On the other hand, the total infrared luminosity can also be

converted to SFR on the assumption of the initial mass function if it is solely generated by star formation (Kennicutt & Evans 2012). We assume that this is the case in H II galaxies. Thus, we can estimate the number of ionizing photons (Q_{IR}) expected from SFR required to explain the total infrared luminosity. Adopting the calibration provided by Murphy et al. (2011), we convert the total infrared luminosity into the number of ionizing photons as

$$Q_{\text{IR}} \text{ (s}^{-1}\text{)} = 5.33 \times 10^9 L_{\text{IR}} \text{ (erg s}^{-1}\text{)}. \quad (3)$$

The $L_{\text{Br}\alpha}/L_{\text{IR}}$ ratio of 2.1×10^{-4} is required to obtain $Q_{\text{Br}\alpha}/Q_{\text{IR}} = 100\%$.

Using Equations (2) and (3), we convert the $L_{\text{Br}\alpha}/L_{\text{IR}}$ ratio into the $Q_{\text{Br}\alpha}/Q_{\text{IR}}$ ratio. We find that the mean $L_{\text{Br}\alpha}/L_{\text{IR}}$ ratio in H II galaxies of 6.9×10^{-5} yields the $Q_{\text{Br}\alpha}/Q_{\text{IR}}$ ratio of only $\sim 33\%$. This indicates that starburst explains merely less than one-third of the total infrared luminosity, even in H II galaxies. This is inconsistent with the assumption that H II galaxies are dominated by starburst. Similar results that the number of ionizing photons derived from the near-infrared hydrogen recombination lines is low relative to that expected from the total infrared luminosity in ULIRGs have been reported by Goldader et al. (1995) using the $\text{Br}\gamma$ line and Valdés et al. (2005) using the $\text{Pa}\alpha$ and $\text{Br}\gamma$ lines. Our result indicates that the $\text{Br}\alpha$ line also suffers the same kind of deficit.

Comparing our result with the *Spitzer* result (Figure 5), we show that $R_{\text{SB}}^{\text{AKARI}}$, which is based on the assumption of 100% contribution of starburst in H II galaxies, is consistent with the fractional contribution of starburst estimated from the longer wavelength result (§4.1.2). This indicates that the apparently low $Q_{\text{Br}\alpha}/Q_{\text{IR}}$ ratio is caused by underestimation of the number of ionizing photons with the $\text{Br}\alpha$ line by a factor of ~ 3 .

As we see in §3.2 with the entire sample, the $\text{Br}\alpha$ line flux could be underestimated by a factor of two due to dust extinction. To closely investigate this effect, we calculate the mean $Q_{\text{Br}\alpha}/Q_{\text{IR}}$ ratio in H II galaxies with correcting $L_{\text{Br}\alpha}$ using $A_V^{9.7}$. We find that the mean $Q_{\text{Br}\alpha}/Q_{\text{IR}}$ ratio increases to 55.5% but is still lower than 100%. The standard error is estimated as 7.5% (1σ), and so the significance of the deviation from 100% is estimated as $\sim 6\sigma$ even after the dust extinction correction with $A_V^{9.7}$. Thus we conclude that the number of ionizing photons traced by the $\text{Br}\alpha$ line is deficient relative to that expected from the total infrared luminosity even taking heavy dust extinction into consideration.

In addition to heavy dust extinction, we propose that dust within the starburst ionized regions absorbs a significant fraction of ionizing photons from OB stars and causes the underestimation of the number of ionizing photons with the $\text{Br}\alpha$ line. If only a fraction $f\%$ of photons with energy > 13.6 eV ionizes the gas while the remaining $(100 - f)\%$ is absorbed by dust, the hydrogen lines underestimate the number of ionizing photons to be $f\%$ of the intrinsic value. Hirashita et al. (2003) have estimated an average value of $(100 - f) \sim 50\%$, with some objects reaching $(100 - f) \sim 80\%$, based on observations of IUE-selected star-forming galaxies. To explain the discrepancy between $Q_{\text{Br}\alpha}$ and Q_{IR} in H II

galaxies after taking the uncertainty of dust extinction into consideration, the fraction of ionizing photons absorbed by dust is required to be $\sim 45\%$, which is well within the range of the possible values indicated by Hirashita et al. (2003). We suggest that the absorption of ionizing photons within H II regions is required in addition to heavy dust extinction to the $\text{Br}\alpha$ line to explain the underestimation of $Q_{\text{Br}\alpha}$ relative to Q_{IR} in ULIRGs.

5. SUMMARY

We conducted systematic observations of the hydrogen $\text{Br}\alpha$ line with the *AKARI* IRC 2.5–5.0 μm spectroscopy in 50 nearby ($z < 0.3$) ULIRGs to estimate the strength of starburst unbiased by dust extinction. We detected the $\text{Br}\alpha$ line in 33 ULIRGs. Comparing the $\text{Br}\alpha$ line with the 3.3 μm PAH emission and the total infrared luminosity, we investigate the fractional contribution of starburst to the total infrared luminosity in ULIRGs. The main results are as follows:

1. The effect of heavy dust extinction to the $\text{Br}\alpha$ line is investigated with the $\text{Br}\beta/\text{Br}\alpha$ line ratio in one source and the optical depth of 9.7 μm silicate absorption taken from *Spitzer* results in the entire sample. We conclude that the intrinsic $\text{Br}\alpha$ line flux is determined within the uncertainty of a factor of two underestimation even if we take the effect of heavy dust extinction into consideration.
2. From the comparison of the $\text{Br}\alpha$ line luminosity ($L_{\text{Br}\alpha}$) with the 3.3 μm PAH emission luminosity ($L_{3.3}$), we find a good correlation between $L_{3.3}$ and $L_{\text{Br}\alpha}$. This indicates that $L_{3.3}$ and $L_{\text{Br}\alpha}$ trace the same excitation sources, i.e., star formation. On the other hand, the total infrared luminosity (L_{IR}) and $L_{\text{Br}\alpha}$ show no clear correlation with each other. Thus a contribution from energy sources other than star formation, i.e., AGN, to L_{IR} is indicated in our sample.
3. To investigate star formation in fainter objects, we derive following relation on the assumption of a proportionality between $L_{3.3}$ and $L_{\text{Br}\alpha}$; $L_{\text{Br}\alpha}/L_{3.3} = 0.177 \pm 0.003$. Using $L_{3.3}$ as an indicator of star formation, we reconfirm that $L_{3.3}$ and L_{IR} show no clear correlation with each other, as well as $L_{\text{Br}\alpha}$ and L_{IR} , in a larger sample of 46 galaxies in which objects with no $\text{Br}\alpha$ line detection are included.
4. The mean $L_{\text{Br}\alpha}/L_{\text{IR}}$ ratio is significantly lower in galaxies optically classified as LINERs and Seyferts than in H II galaxies. This difference is also confirmed with the $L_{3.3}/L_{\text{IR}}$ ratio in the larger sample. We propose that the difference reflects the contribution of starburst to the total infrared luminosity in ULIRGs. Assuming that H II galaxies are 100% energized by starburst, we estimate that the contribution of starburst to the total infrared luminosity in LINERs and Seyferts is $\sim 67\%$, and active galactic nuclei contribute to the remaining $\sim 33\%$.
5. We find that the number of ionizing photons derived from the $\text{Br}\alpha$ line ($Q_{\text{Br}\alpha}$) are significantly smaller than that expected from star formation rate

required to explain the total infrared luminosity (Q_{IR}). The mean $L_{\text{Br}\alpha}/L_{\text{IR}}$ ratio in H II galaxies yields the $Q_{\text{Br}\alpha}/Q_{\text{IR}}$ ratio of only $55.5 \pm 7.5\%$ even after taking heavy dust extinction into consideration. We attribute this apparently low ratio to the underestimation of the number of ionizing photons with the $\text{Br}\alpha$ line. We conclude that the number of ionizing photons traced by the $\text{Br}\alpha$ line is deficient relative to that expected from the total infrared luminosity even taking the effect of heavy dust extinction into consideration. As an additional cause of the deficit, we propose that dust within H II regions absorbs a significant fraction ($\sim 45\%$) of ionizing photons.

This work is based on the observations made with *AKARI*, a JAXA project, with the participation of ESA. This research also made use of the NASA/IPAC Extragalactic Database, which is operated by the Jet Propulsion Laboratory, California Institute of Technology, under contract with the National Aeronautics and Space Administration. We thank the anonymous referee for his/her useful comments which significantly improved this paper. This work is supported by JSPS KAKENHI Grant Number 26247030. K.Y. is supported through the Leading Graduates Schools Program, gAdvanced Leading Graduate Course for Photon Science, by the Ministry of Education, Culture, Sports, Science and Technology of Japan.

Facility: Akari (IRC)

REFERENCES

- Abazajian, K., Adelman-McCarthy, J. K., Agüeros, M. A., et al. 2003, *AJ*, 126, 2081
— 2005, *AJ*, 129, 1755
Adelman-McCarthy, J. K., Agüeros, M. A., Allam, S. S., et al. 2006, *ApJS*, 162, 38
— 2008, *ApJS*, 175, 297
Alonso-Herrero, A., Pereira-Santaella, M., Rieke, G. H., & Rigopoulou, D. 2012, *ApJ*, 744, 2
Armus, L., Heckman, T. M., & Miley, G. K. 1989, *ApJ*, 347, 727
Armus, L., Charmandaris, V., Bernard-Salas, J., et al. 2007, *ApJ*, 656, 148
Baldwin, J. A., Phillips, M. M., & Terlevich, R. 1981, *PASP*, 93, 5
Buchanan, C. L., McGregor, P. J., Bicknell, G. V., & Dopita, M. A. 2006, *AJ*, 132, 27
Carilli, C. L., Wrobel, J. M., & Ulvestad, J. S. 1998, *AJ*, 115, 928
Colless, M., Dalton, G., Maddox, S., et al. 2001, *MNRAS*, 328, 1039
Colless, M., Peterson, B. A., Jackson, C., et al. 2003, *arXiv:astro-ph/0306581*
Dale, D. A., & Helou, G. 2002, *ApJ*, 576, 159
Darling, J., & Giovanelli, R. 2006, *AJ*, 132, 2596
Dartois, E., & Muñoz-Caro, G. M. 2007, *A&A*, 476, 1235
Downes, D., Solomon, P. M., & Radford, S. J. E. 1993, *ApJL*, 414, L13
Draine, B. T. 2003, *ARA&A*, 41, 241
Duc, P.-A., Mirabel, I. F., & Maza, J. 1997, *A&AS*, 124, 533
Fisher, K. B., Huchra, J. P., Strauss, M. A., et al. 1995, *ApJS*, 100, 69
Fritz, T. K., Gillessen, S., Dodds-Eden, K., et al. 2011, *ApJ*, 737, 73
Genzel, R., Lutz, D., Sturm, E., et al. 1998, *ApJ*, 498, 579
Goldader, J. D., Joseph, R. D., Doyon, R., & Sanders, D. B. 1995, *ApJ*, 444, 97
Hirashita, H., Buat, V., & Inoue, A. K. 2003, *A&A*, 410, 83
Ho, L. C. 2008, *ARA&A*, 46, 475
Hou, L. G., Wu, X.-B., & Han, J. L. 2009, *ApJ*, 704, 789
Huchra, J., Davis, M., Latham, D., & Tonry, J. 1983, *ApJS*, 52, 89
Hwang, H. S., Serjeant, S., Lee, M. G., Lee, K. H., & White, G. J. 2007, *MNRAS*, 375, 115
Imanishi, M. 2009, *ApJ*, 694, 751
Imanishi, M., Dudley, C. C., Maiolino, R., et al. 2007, *ApJS*, 171, 72
Imanishi, M., Maiolino, R., & Nakagawa, T. 2010a, *ApJ*, 709, 801
Imanishi, M., Nakagawa, T., Ohya, Y., et al. 2008, *PASJ*, 60, 489
Imanishi, M., Nakagawa, T., Shirahata, M., Ohya, Y., & Onaka, T. 2010b, *ApJ*, 721, 1233
Jones, D. H., Saunders, W., Colless, M., et al. 2004, *MNRAS*, 355, 747
Jones, D. H., Read, M. A., Saunders, W., et al. 2009, *MNRAS*, 399, 683
Kennicutt, R. C., & Evans, N. J. 2012, *ARA&A*, 50, 531
Kim, D.-C., & Sanders, D. B. 1998, *ApJS*, 119, 41
Kim, D.-C., Veilleux, S., & Sanders, D. B. 1998, *ApJ*, 508, 627
Kim, J. H., Im, M., Lee, H. M., et al. 2012, *ApJ*, 760, 120
Komatsu, E., Smith, K. M., Dunkley, J., et al. 2011, *ApJS*, 192, 18
Lauberts, A., & Valentijn, E. A. 1989, *The Surface Photometry Catalogue of the ESO-Uppsala Galaxies* (Garching, Germany: European Southern Observatory)
Lipari, S., Colina, L., & Macchetto, F. 1994, *ApJ*, 427, 174
Lorente, R., Onaka, T., Ita, Y., et al. 2008, *AKARI IRC Data User Manual* (Version 1.4), <http://www.ir.isas.jaxa.jp/ASTRO-F/Observation/DataReduction/IRC/>
Mirabel, I. F., Lutz, D., & Maza, J. 1991, *A&A*, 243, 367
Moshir, M., Kopman, G., & Conrow, T. A. O. 1992, *IRAS Faint Source Survey*, Explanatory Supplement Version 2 (Pasadena, CA: California Institute of Technology)
Murakami, H., Baba, H., Barthel, P., et al. 2007, *PASJ*, 59, 369
Murphy, E. J., Condon, J. J., Schinnerer, E., et al. 2011, *ApJ*, 737, 67
Murphy, Jr., T. W., Soifer, B. T., Matthews, K., Armus, L., & Kiger, J. R. 2001, *AJ*, 121, 97
Nagar, N. M., Wilson, A. S., Falcke, H., Veilleux, S., & Maiolino, R. 2003, *A&A*, 409, 115
Nardini, E., Risaliti, G., Salvati, M., et al. 2009, *MNRAS*, 399, 1373
Ohya, Y., Onaka, T., Matsuhara, H., et al. 2007, *PASJ*, 59, 411
Onaka, T., Matsuhara, H., Wada, T., et al. 2007, *PASJ*, 59, 401
Osterbrock, D. E., & Ferland, G. J. 2006, *Astrophysics of Gaseous Nebulae and Active Galactic Nuclei* (2nd ed.; Sausalito, CA: University Science Books)
Prouton, O. R., Bressan, A., Clemens, M., et al. 2004, *A&A*, 421, 115
Rothberg, B., & Joseph, R. D. 2006, *AJ*, 131, 185
Rupke, D. S. N., Veilleux, S., & Baker, A. J. 2008, *ApJ*, 674, 172
Sanders, D. B., Egami, E., Lipari, S., Mirabel, I. F., & Soifer, B. T. 1995, *AJ*, 110, 1993
Sanders, D. B., Mazzarella, J. M., Kim, D.-C., Surace, J. A., & Soifer, B. T. 2003, *AJ*, 126, 1607
Sanders, D. B., & Mirabel, I. F. 1996, *ARA&A*, 34, 749
Sanders, D. B., Soifer, B. T., Elias, J. H., et al. 1988, *ApJ*, 325, 74
Shipley, H. V., Papovich, C., Rieke, G. H., et al. 2013, *ApJ*, 769, 75
Strauss, M. A., & Huchra, J. 1988, *AJ*, 95, 1602
Strauss, M. A., Huchra, J. P., Davis, M., et al. 1992, *ApJS*, 83, 29
Valdés, J. R., Berta, S., Bressan, A., et al. 2005, *A&A*, 434, 149
Veilleux, S., Kim, D.-C., & Sanders, D. B. 1999, *ApJ*, 522, 113
Veilleux, S., Kim, D.-C., Sanders, D. B., Mazzarella, J. M., & Soifer, B. T. 1995, *ApJS*, 98, 171
Veilleux, S., & Osterbrock, D. E. 1987, *ApJS*, 63, 295
Veilleux, S., Sanders, D. B., & Kim, D.-C. 1997, *ApJ*, 484, 92
Veilleux, S., Rupke, D. S. N., Kim, D.-C., et al. 2009, *ApJS*, 182, 628
Willett, K. W., Darling, J., Spoon, H. W. W., Charmandaris, V., & Armus, L. 2011, *ApJS*, 193, 18
Wu, Y., Charmandaris, V., Huang, J., Spinoglio, L., & Tommasin, S. 2009, *ApJ*, 701, 658
Yamada, R., Oyabu, S., Kaneda, H., et al. 2013, *PASJ*, 65, 103
York, D. G., Adelman, J., Anderson, Jr., J. E., et al. 2000, *AJ*, 120, 1579